Neuron
Article

Homeostatic Regulation of Synaptic GlyR Numbers Driven by Lateral Diffusion

Sabine Lévi,[1,2] Claude Schweizer,[1] Hiroko Bannai,[1,3] Olivier Pascual,[1] Cécile Charrier,[1] and Antoine Triller[1,*]
[1]Biologie Cellulaire de la Synapse, INSERM U789, Ecole Normale Supérieure, 46 rue d'Ulm, 75005 Paris, France
[2]Present address: Plasticity in Cortical Networks & Epilepsy, INSERM UMR-839, Institut du Fer à Moulin, 17 rue du Fer à Moulin, 75005 Paris, France
[3]Present address: Laboratory for Developmental Neurobiology, Brain Science Institute, RIKEN, Saitama 351-0198, Japan
*Correspondence: triller@biologie.ens.fr
DOI 10.1016/j.neuron.2008.05.030

SUMMARY

In the spinal cord, most inhibitory synapses have a mixed glycine-GABA phenotype. Using a pharmacological approach, we report an NMDAR activity-dependent regulation of the mobility of GlyRs but not $GABA_A$Rs at inhibitory synapses in cultured rat spinal cord neurons. The NMDAR-induced decrease in GlyR lateral diffusion was correlated with an increase in receptor cluster number and glycinergic mIPSC amplitude. Changes in GlyR diffusion properties occurred rapidly and before the changes in the number of synaptic receptors. Regulation of synaptic GlyR content occurred without change in the amount of gephyrin. Moreover, NMDAR-dependent regulation of GlyR lateral diffusion required calcium influx and calcium release from stores. Therefore, excitation may increase GlyR levels at synapses by a calcium-mediated increase in postsynaptic GlyR trapping involving regulation of receptor-scaffold interactions. This provides a mechanism for a rapid homeostatic regulation of the inhibitory glycinergic component at mixed glycine-GABA synapses in response to increased NMDA excitatory transmission.

INTRODUCTION

The inhibitory amino acids glycine and GABA are coreleased from single vesicles at interneuron-motoneuron synapses (Jonas et al., 1998). In the postsynaptic differentiation (PSD), glycine receptors (GlyR) and type A GABAR ($GABA_A$R) immunoreactivities (IRs) are associated with gephyrin (Bohlhalter et al., 1994; Todd et al., 1996; Colin et al., 1998; Dumoulin et al., 2000). Gephyrin is the core scaffold protein responsible for the postsynaptic clustering of GlyR (Kirsch et al., 1993; Feng et al., 1998; Levi et al., 2004) and $GABA_A$R subtypes (Essrich et al., 1998; Kneussel et al., 1999, 2001; Levi et al., 2004; Jacob et al., 2005; Tretter et al., 2008). Interestingly, GlyR clustering is regulated by GlyR activation and neuronal activity (Kirsch and Betz, 1998; Levi et al., 1998; Gonzalez-Forero and Alvarez, 2005). In the brain, inhibitory GABAergic synapses undergo homeostatic regulation: the blockade of spiking synaptic activity with tetrodotoxin (TTX) for 48 hr decreases the amplitude of inhibitory GABA mIPSCs (Kilman et al., 2002). Epilepsy models that increase excitatory activity increase the amplitude and frequency of GABA mIPSCs (Wierenga and Wadman, 1999; Otis et al., 1994; Nusser et al., 1998). In most cases, synaptic scaling of inhibitory synapses is achieved by changing the number of $GABA_A$Rs clustered at synaptic sites (Nusser et al., 1998; Kilman et al., 2002). In previous experiments, this regulation required hours to days (Turrigiano et al., 1998). Receptor movements in and out of synapses could constitute the molecular basis of the adaptative regulation of receptor number at synapses. Electrophysiology and single-molecule imaging experiments have revealed that neurotransmitter receptors (NTRs) are constantly exchanged from the extrasynaptic plasma membrane to synaptic sites by means of lateral diffusion (Choquet and Triller, 2003; Triller and Choquet, 2005). This occurs for GlyR and $GABA_A$R (Meier et al., 2001; Thomas et al., 2005; Bogdanov et al., 2006) and also for the excitatory glutamate receptors (Borgdorff and Choquet, 2002; Tovar and Westbrook, 2002; Tardin et al., 2003; Groc et al., 2004). Immobilization and subsequent accumulation of receptors at synaptic sites result from interactions with molecular scaffolds that link membrane receptors to the cytoskeleton. Interactions with the major PSD scaffolding molecules gephyrin, Homer, and PSD-95 favor the confinements of GlyRs, mGluRs, and AMPARs, respectively (Meier et al., 2001; Serge et al., 2002; Bats et al., 2007). Membrane AMPAR dynamics are regulated during synapse formation (Borgdorff and Choquet, 2002) and by activity (Tardin et al., 2003; Groc et al., 2004; Ehlers et al., 2007). We report activity and calcium dependence of GlyR but not $GABA_A$R mobility, accumulation at synapses, and glycinergic miniature currents. This provides a rapid homeostasis of excitation-inhibition balance through tuning of GlyR numbers at mixed inhibitory synapses.

RESULTS

Differences in GlyR and $GABA_A$R Clustering and Diffusion Properties

GlyR and $GABA_A$R localization at synapses was investigated in spinal cord neurons cultured for 10–13 days in vitro (DIV) with triple-immunolabeling experiments using antibodies against the adult GlyRα1 subunit, the $GABA_A$Rγ2 subunit, and VIAAT, a presynaptic marker of inhibitory terminals. As shown previously (e.g., Dumoulin et al., 2000; Muller et al., 2006), GlyRα1 and

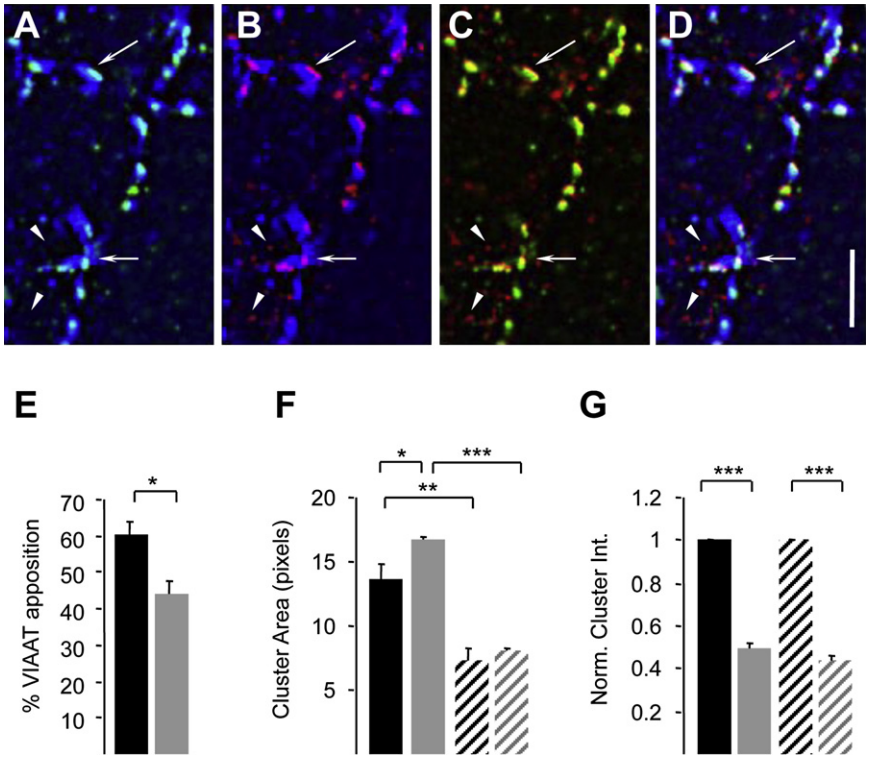

Figure 1. GlyR and $GABA_AR$ Clustering at Inhibitory Synapses

(A–D) Spinal cord neurons at DIV10–13 triple-stained for GlyRα1 subunit (green), $GABA_AR\gamma2$ subunit (red), and VIAAT (blue). Detection of (A) GlyRα1 and VIAAT, (B) $GABA_AR\gamma2$ and VIAAT, (C) GlyRα1 and $GABA_AR\gamma2$, and (D) GlyRα1, $GABA_AR\gamma2$, and VIAAT. Arrows, colocalized elements; arrowheads, extrasynaptic $GABA_AR\gamma2$ clusters not associated with GlyRα1. Scale bar, 5 μm.

(E) Percentage of GlyRα1 (black) and $GABA_AR\gamma2$ (gray) clusters apposed to VIAAT-IR profiles.

(F and G) Averaged surface area (F) and normalized fluorescence intensities (G) of GlyRα1 (black) and $GABA_AR\gamma2$ (gray) clusters apposed (plain) or not (hatched) to VIAAT-IR terminals. Cluster size and fluorescence intensities of synaptic receptors are more than 2-fold (***$p < 10^{-3}$, t test) those of extrasynaptic ones. GlyRα1 and $GABA_AR\gamma2$ cluster fluorescence intensities were normalized to the averaged fluorescence intensity of the corresponding synaptic clusters.

In all graphs, values are mean ± SEM; *$p < 5\ 10^{-2}$, **$p < 10^{-2}$, ***$p < 10^{-3}$, t test.

$GABA_AR\gamma2$ subunits formed numerous clusters over somata and neurites (Figures 1A–1D). The immunofluorescence associated with GlyR was mainly located at synapses (Figure 1A). $GABA_AR$ clusters were also found at synapses but with a lower frequency than GlyR clusters. About 80% (79.7 ± 2.2, n cells = 40, 3 independent cultures) of the synaptic GlyR clusters also contained $GABA_AR$-IR (Figures 1C and 1D). $GABA_AR$ also formed small nonsynaptic clusters distant from synaptic sites, and most of them did not colocalize with GlyR-IR (arrowheads in Figures 1A–1D). Quantifications indicated that 60.6% ± 3.2% and 44.1% ± 3.8% of GlyR-IR and $GABA_AR$-IR clusters were apposed to VIAAT-IR inhibitory synapses (Figure 1E). At inhibitory synapses, the average surface areas (Figure 1F) and fluorescence intensities (Figure 1G) of GlyR- and $GABA_AR$-IR clusters were ~2-fold that of extrasynaptic clusters of receptors ($p < 10^{-3}$; t test). The surface area of postsynaptic $GABA_AR$-IR clusters was slightly but significantly (~1.23-fold) larger than that of GlyR-IR clusters (Figure 1F; $p = 5\ 10^{-2}$; t test). This suggests that, at mixed inhibitory synapses, GlyRs are restricted to the active zone while $GABA_ARs$ may extend beyond it or that GlyRs occupy a subdomain of the PSD while $GABA_ARs$ are distributed over the whole PSD.

We analyzed GlyR and $GABA_AR$ lateral diffusion using the single-particle tracking (SPT) technique as previously described (Dahan et al., 2003; Bannai et al., 2006). Neurons were surface labeled at DIV10–13 for the GlyRα1 subunit or the $GABA_AR\gamma2$ subunit with quantum dot (QD)-coupled antibodies. QDs were classified as synaptic upon colocalization with active presynaptic terminals loaded with FM4-64 (e.g., Figure 2B). In this experimental model, inhibitory synapses represent ~70% of the total number of synapses (Dumoulin et al., 2000). QD exploratory maps obtained from projections of image sequences indicated that GlyR-QD and $GABA_AR$-QD diffused over broad areas of the extrasynaptic plasma membrane (Figures 2A and 2C). In contrast, the receptor-QD exploratory map was reduced at synapses (e.g., GlyR-QD; Figure 2B). It corresponds to receptor diffusion above gephyrin clusters (Charrier et al., 2006). As shown previously for GlyR (Dahan et al., 2003), $GABA_AR$-QD could exchange between extrasynaptic and synaptic compartments (Figure 2C). QD trajectories (e.g., insets in Figures 2D and 2E corresponding to QDs shown in Figures 2A and 2B and Figure 2C, respectively) were reconstructed with custom software (Bonneau et al., 2005). The plots of mean-square displacement function (MSD) versus time for GlyR-QDs and $GABA_AR$-QDs were linear and negatively bent in the extrasynaptic and synaptic membrane, respectively (Figures 2D and 2E corresponding to GlyR and $GABA_AR$-QD). As exemplified (Figure 2F) for the $GABA_AR$ (same trajectory as the inset in Figure 2E), the instantaneous diffusion coefficient (D) of the QD was ~10-fold slower within the synaptic area. Moreover, the instantaneous D fluctuated ~20-fold more in the extrasynaptic (variance = $17\ 10^{-4}$ $(\mu m^2 s^{-1})^2$) than in the synaptic (variance = $0.9\ 10^{-4}$ $(\mu m^2 s^{-1})^2$) compartment. These variations likely reflect membrane heterogeneity or local molecular interactions. Pooling the data from many QDs gives access to the behavior of receptor populations. For GlyRs (Figure 2G) as well as for $GABA_ARs$ (Figure 2H), extrasynaptic QDs (GlyR, n = 351; $GABA_AR$, n = 437; 3 cultures) were more mobile than synaptic QDs (GlyR, n = 336; $GABA_AR$, n = 264; $p < 10^{-3}$, Kolmogorov-Smirnov KS test). In the case of GlyRs, two different antibodies (monoclonal and polyclonal)

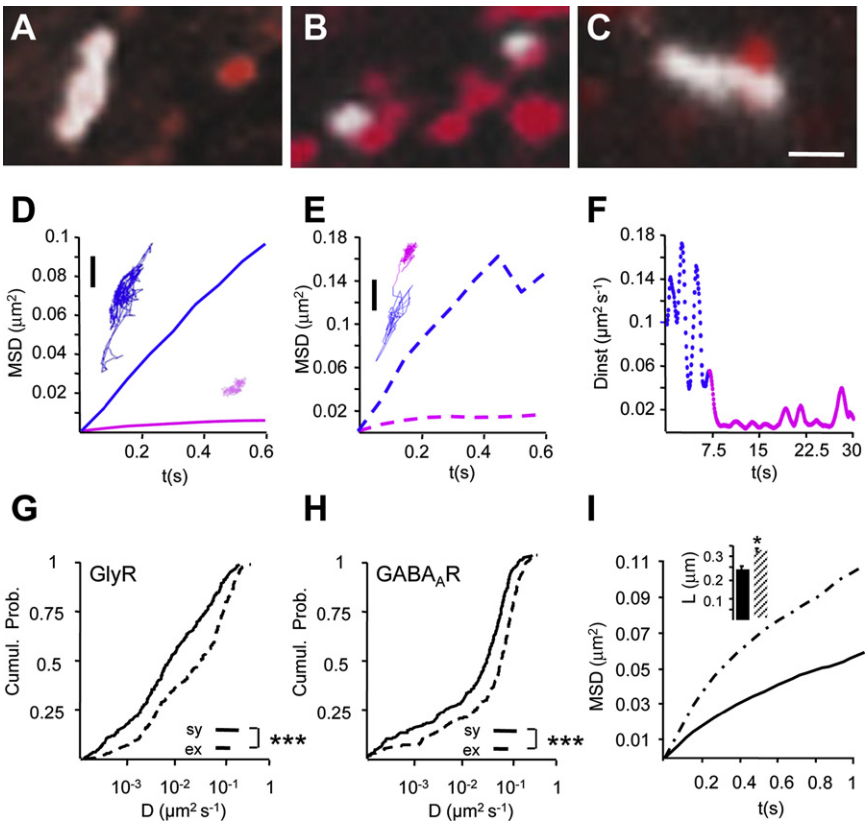

Figure 2. GlyR and $GABA_AR$ Diffusion Properties

(A–C) Examples of surface exploration by itinerant GlyR-QDs (A and B) and $GABA_AR$-QD (C) visualized on maximum intensity projections of images (GlyR-QDs, 512 frames; $GABA_AR$-QD, 400 frames). QD trajectories and FM4-64-stained synapses are white and red, respectively. (A and B) Larger surface area explored by GlyR-QDs outside (A) than at synapses (B); (C) $GABA_AR$-QDs diffusing in and out of synapses. Scale bar, 1 μm.

(D and E) Time-averaged MSD function of QDs shown in (A)–(C). (D) Curves corresponding to individual extrasynaptic (blue, 512 frames) and synaptic (pink, 512 frames) GlyR-QDs connected trajectories in (A) and (B), respectively (insets in [D], same color code). (E) Curves corresponding to the $GABA_AR$-QD trajectory in (C). Same representation as in (D) (91 extrasynaptic and 307 synaptic frames of the same trajectory, inset). Scale bars, 0.5 μm. Extrasynaptic and synaptic QDs display linear and negatively bent MSD curves, characteristic of random walk and confined movement, respectively.

(F) Instantaneous diffusion coefficients of the $GABA_AR$-QD shown in (C) (extrasynaptic and synaptic, blue and pink, respectively). Note the drop of the QD diffusion coefficient and the reduction in its fluctuations when entering the synapse.

(G and H) Comparison of synaptic (plain) and extrasynaptic (hatched) receptors. Cumulative probabilities of GlyR-QDs (G) and $GABA_AR$-QDs (H) diffusion coefficients. Note that GlyR-QDs and $GABA_AR$-QDs are slower at synapses than in extrasynaptic regions (***$p < 10^{-3}$, KS test).

(I) Comparison of GlyR and $GABA_AR$ confinements at synapses. Average MSD as a function of time at synaptic loci. The shape of the MSD curve indicates a greater restriction in movement for GlyR-QDs (black) than for $GABA_AR$-QDs (hatched). Inset, confinement domain L (average ± SEM). Note that $GABA_AR$-QDs (hatched) explore a broader synaptic area than GlyR-QDs (black) (*$p < 5\ 10^{-2}$, t test).

were used, and similar values were obtained for D inside and outside synapses as well as for synaptic confinement (see Figure S1 available online). The adhesion molecule N-Cam, which does not accumulate at synapses, moves ~25-fold faster than GlyRs at synapses (Figure S2). The shape of the MSD versus time curves at synapses was different for GlyR-QDs and $GABA_AR$-QDs, indicating a stronger confinement for GlyR than for $GABA_AR$ (Figure 2I). This was further illustrated (inset in Figure 2I) by a larger confinement domain (L) for $GABA_AR$-QDs than for GlyR-QDs ($GABA_AR$, L = 318.4 ± 20.1 nm; n = 116; GlyR, L = 237.2 ± 17.7 nm; n = 116; p = 0.027; t test). This parameter characterizes the exploratory capacity of a given particle per unit time and therefore reflects the molecular crowding and the density of binding sites limiting diffusion. This means that $GABA_AR$-QDs explored a larger surface area of the synaptic membrane than GlyR-QDs and consequently tended to escape more easily from the synaptic domain.

Synaptic Transmission Controls GlyR Lateral Diffusion

Calcium fluctuations that reflect neuronal activity were monitored using time-lapse recording of cultured neurons loaded with the cell permeant Fluo4-AM Ca^{2+} dye. The K_d (100–500 nM) of Fluo4-AM is compatible with the detection of fluctuations in cytoplasmic free Ca^{2+}, which is plotted here as the F/F0 ratio at each recording time point (Figure 3A). A few seconds after application of 1 μM TTX, the Ca^{2+} level decreased in all cells analyzed (Figure 3A), to 64.6% ± 1.6% of the control values (n cells = 62; 3 cultures; $p < 10^{-3}$; Mann-Whitney U test). These cultured spinal neurons therefore displayed background synaptic neuronal activity that could be blocked by TTX. We then analyzed the impact of synaptic activity on GlyR-QD lateral diffusion. In untreated cultures, GlyR-QD instantaneous D were low, with small fluctuations. After TTX treatment, these increased dramatically. This is exemplified in Figure 3B for two QDs in the absence (black and gray) and two QDs in the presence (red and pink) of TTX. Following TTX treatment, the variance increased dramatically from 0.3–0.5 10^{-3} $(\mu m^2 s^{-1})^2$ to 11–53 10^{-3} $(\mu m^2 s^{-1})^2$. Global measurements indicated that TTX significantly increased, by ~2.3-fold, the median D of GlyR-QDs (Figure 3C; Ctr, n = 723; TTX, n = 635; 3 cultures; $p < 10^{-3}$; KS test) but not $GABA_AR$-QDs (Figure 3D; Ctr, n = 551; TTX, n = 736; 3 cultures; p > 0.99; KS test). Increasing neuronal activity with GlyR and $GABA_AR$ antagonists strychnine (1 μM) and SR-95531 (5 μM) had the opposite effect on GlyR diffusion dynamics. In the presence of strychnine and SR-95531, GlyR-QD D were lower (~5.1-fold) than those measured in untreated neurons (Figure 3E; Ctr, n = 865;

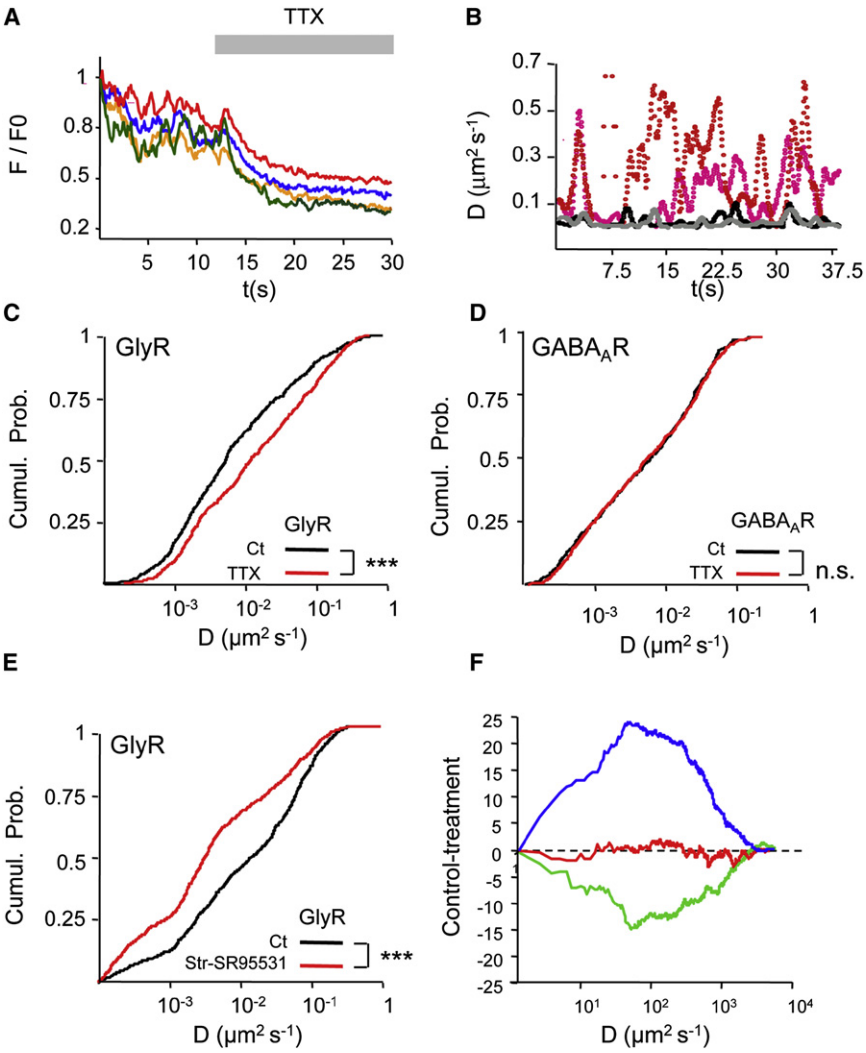

Figure 3. Activity Modifies GlyR but Not $GABA_AR$ Membrane Diffusion

(A) Four examples of calcium level changes shown as the F/F0 ratio measured as a function of time on proximal dendrites following TTX (1 μM) application (gray bar).

(B) Examples of individual GlyR-QD instantaneous diffusion coefficients in the absence (black and gray) or presence (red and pink) of TTX. Note that TTX treatment increases GlyR-QDs diffusion coefficients and fluctuations.

(C and D) Cumulative probabilities of GlyR-QDs (C) and $GABA_AR$-QDs (D) diffusion coefficients at the neuronal surface. Note that TTX increases the GlyR-QDs diffusion coefficient (***$p < 10^{-3}$, KS test) but not that of $GABA_AR$-QDs (n.s., not significant).

(E) Strychnine (1 μM) and SR-95531 (5 μM) decrease GlyR-QDs lateral diffusion. Cumulative probabilities of GlyR-QDs diffusion coefficients in the absence (black) or presence (red) of inhibitory receptor antagonists (***$p < 10^{-3}$, KS test).

(F) Subtraction histograms calculated from the cumulative distributions in (C) (control-TTX for GlyR, green), (D) (control-TTX for $GABA_AR$, red), and (E) (control-Stry+SR-95531 for GlyR, blue), emphasizing the influence of activity on GlyR-QDs but not on $GABA_AR$-QDs diffusion coefficients (see text for explanation). Positive and negative values indicate increased or reduced diffusion rate.

Str-SR-95531, n = 890; 3 cultures; $p < 10^{-3}$; KS test). Subtraction curves (control minus treatment) emphasize that strychnine-SR-95531 and TTX treatments reduced and increased, respectively, GlyR-QD diffusion but that TTX had no effect on $GABA_AR$-QD diffusion (Figure 3F). The dynamics of N-Cam were not modified by TTX treatment (Figure S2). Therefore, changes in GlyR activity-dependent diffusion do not result from a nonspecific action on the plasma membrane. These results indicate that GlyR but not $GABA_AR$ diffusion depends on Na^+ channel-dependent neuronal activity.

NMDARs Control GlyR but Not $GABA_AR$ Lateral Diffusion

Spinal cord neurons express functional excitatory AMPARs and NMDARs in culture (O'Brien et al., 1998). The mobility of inhibitory receptors was measured after acute blockade of AMPARs and NMDARs with CNQX (50 μM) and D-AP5 (50 μM). This treatment rapidly decreased the intracellular calcium concentration in all cells analyzed, indicating a reduction in synaptic activity (Figure 4A). The Fluo4-AM F/F0 ratio rapidly decreased by 68.8% ± 1.7% compared with control (n cells = 68; 3 cultures; $p < 10^{-3}$; Mann-Whitney U test) after addition of the drugs (Figure 4B), and this reduction lasted as long as the antagonists were applied. This indicated that excitatory transmission increased $Ca^{2+}{}_i$ in DIV10–12 spinal neurons. The block of excitatory receptors increased the lateral diffusion of GlyR-QDs (Figure 4C) but not of $GABA_AR$-QDs (Figure 4D). The median GlyR-QDs D increased following exposure to D-AP5 and CNQX, to D-AP5 alone, but not to CNQX alone (Figure S3). This suggested that NMDARs but not AMPARs controlled GlyR lateral diffusion. Moreover, the block of L-type voltage-dependent Ca^{2+} channels with nifedipine (25 μM) significantly increased the median GlyR-QDs D, indicating that GlyR mobility depends on cell depolarization (Figure S3). Therefore, the lateral diffusion of GlyRs but not $GABA_ARs$ is modulated by NMDAR activation.

NMDA-Induced Slowing of GlyRs

Neurons were acutely exposed to the agonist NMDA (50 μM, a value close to the EC_{50} = 30–35 μM; Patneau and Mayer, 1990; Buller et al., 1994) and the coagonist glycine (5 μM) in the presence of TTX (1 μM; "NMDA condition"). We compared cultures treated with the NMDA condition to cultures treated with TTX and glycine only ("TTXgly condition"; Figure 5). In the presence of NMDA, GlyR-QD D were lower (~4.5-fold) than those measured in TTXgly-treated neurons (Figure 5A; TTXgly, n = 492; NMDA, n = 579; 3 cultures; $p < 10^{-3}$; KS test). Similar

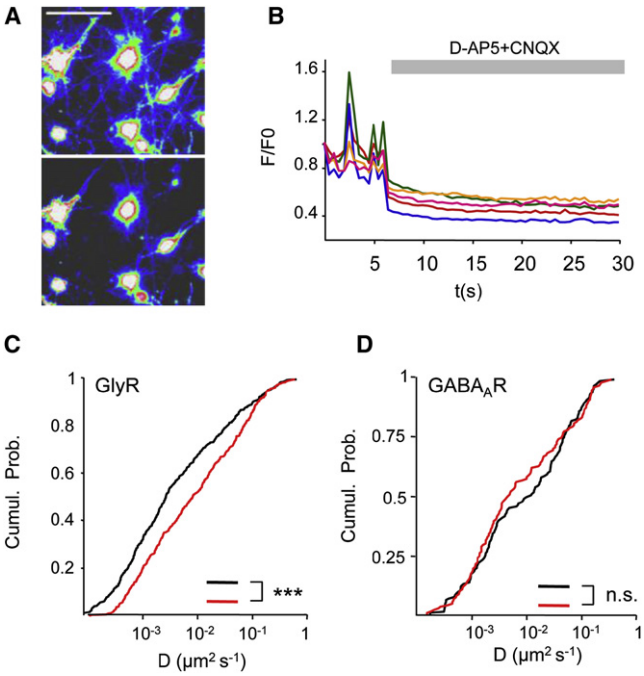

Figure 4. D-AP5 and CNQX Increase GlyR but Not $GABA_AR$ Lateral Mobility

(A) Pseudocolor images of neurons loaded with Fluo4-AM, before (top) and after (bottom) D-AP5 (50 μM) + CNQX (50 μM) treatment. The warmer the color is, the higher is the Fluo4-AM fluorescence intensity. Scale bar, 20 μm.

(B) Five examples of calcium level shown as F/F0 ratio measured as a function of time on proximal dendrites following D-AP5 + CNQX application (gray bar).

(C and D) Cumulative probabilities of GlyR-QDs (C) and $GABA_AR$-QDs (D) diffusion coefficients in control (black) and D-AP5 + CNQX (red) conditions. n.s., not significant, ***$p < 10^{-3}$; KS test. Note that D-AP5 + CNQX significantly increases GlyR-QDs but not $GABA_AR$-QDs mobility.

results were obtained when neurons were exposed to 50 μM NMDA or to lower concentration (5 μM; Figure S4). In contrast, NMDAR activation had no effect on N-Cam diffusion (Figure S5). The specific NMDAR antagonist D-AP5 inhibited the NMDA-induced decrease in GlyR-QD D (D-AP5, n = 295; 3 cultures). The cumulative distributions of GlyR-QD D measured in TTXgly and D-AP5 conditions were superimposable (Figure 5A). The effect of NMDA was rapid (within 10 min; Figure S6) and reversible within 10 min (Figure 5A, inset; TTXgly, n = 636; NMDA, n = 882; reversibility, n = 523; 3 cultures; $p < 10^{-3}$; KS test). The NMDA effect on GlyR-QD diffusion was observed at both extrasynaptic and synaptic loci (Figure 5B). The MSD versus time curves for GlyR-QDs were shifted to the right (slower diffusion) and were more negatively bent (greater confinement) in both extrasynaptic (Figure 5C) and synaptic membranes (Figure 5D). This was further evidenced by a reduction in the mean size of the confinement domain L after NMDA treatment (inset in Figure 5D; calculated for receptors remaining at synapses during the entire recording; TTXgly, L = 153 ± 17 nm; n = 114; NMDA, L = 118 ± 10 nm; n = 112; p = 0.036; KS test). These data indicated that, at synapses, GlyR exploration capability was restricted to a smaller surface area in the presence of NMDA compared with TTXgly. This change in diffusion properties was reflected by a change in GlyR-QD exploratory behaviors, as seen on image projections (Figure 5E). NMDA treatment reduced the exploratory behavior of GlyR-QDs in both extrasynaptic and synaptic membranes. In contrast, $GABA_AR$ exploratory maps were not modified following NMDAR activation (not shown but similar to Figure 2B). This was due to the fact that the diffusion properties were not affected by this treatment. Although higher than for GlyR-QDs, $GABA_AR$ median diffusion was unchanged after NMDA or D-AP5 treatment (Figure 5F; TTXgly, D median = 9.3 $10^{-2}\mu m^2 s^{-1}$; n = 349; NMDA, D median = 10.3 $10^{-2}\mu m^2 s^{-1}$; n = 401; 3 cultures; p = 0.46; KS test). In conclusion, NMDA reversibly affected GlyR but not $GABA_AR$ diffusion properties.

Involvement of Excitatory Activity in the Clustering of Inhibitory Receptors

GlyR, $GABA_AR$, and gephyrin amount at synapses were quantified following immunostaining (Figure 6A). We compared cultures treated for 2 hr with the NMDA condition to cultures treated with the TTXgly condition. NMDA increased GlyR cluster immunoreactivity (IR) in nonpermeabilized (GlyRnp) and permeabilized (GlyRp) neurons. In contrast, changes for $GABA_AR$ and gephyrin cluster IR were much smaller. GlyR, $GABA_AR$, and gephyrin levels were quantified by measuring the integrated fluorescence intensity of the corresponding clusters. As exemplified in Figure 6B for one culture, the distribution of GlyR cluster fluorescence intensities was shifted to higher values after 2 hr of NMDA treatment (TTXgly, n clusters = 3458; NMDA, n clusters = 3392; 10 cells from 1 representative culture; $p < 10^{-3}$; KS test). In the same GlyR and $GABA_AR$ double-staining experiment, NMDA treatment did not increase $GABA_AR$ cluster fluorescence intensity (TTXgly, n clusters = 2301; NMDA, n clusters = 2513; $p < 10^{-3}$; KS test). Cell by cell analysis (Figure 6C) revealed that, after NMDA treatment, GlyR cluster-associated fluorescence was 121.7% ± 3.3% of that measured in cells maintained in TTXgly condition in permeabilized neurons (TTXgly, n cells = 194; NMDA, n cells = 201; 9 cultures; $p < 10^{-3}$; t test). It was 137.0% ± 5.8% in nonpermeabilized neurons (TTXgly, n cells = 52; NMDA, n cells = 51; 3 cultures; $p < 10^{-3}$; t test). $GABA_AR$-IR and gephyrin-IR clusters remained unaffected by NMDA treatment ($GABA_AR$: TTXgly, n cells = 84; NMDA, n cells = 85; gephyrin: TTXgly, n cells = 105; NMDA, n cells = 105; 3 cultures). Therefore, GlyRα1 but not $GABA_AR\gamma 2$ and gephyrin levels are increased at synapses after NMDAR activation. The NMDA-induced increase in GlyR-IR without changes in gephyrin-IR suggests that scaffold-receptor rather than scaffold-cytoskeleton interactions are implicated in the regulation of GlyR levels at synapses. The changes in GlyR-IR were seen ~10 min after the effects on diffusion were first observed (Figure S6).

NMDA-Induced Increase in Glycinergic but Not GABAergic mIPSC Amplitude

We then examined glycinergic and GABAergic mIPSCs following NMDA treatment. To avoid GlyRs desensitization, electrophysiology experiments were performed in absence of exogenous glycine. To match electrophysiological conditions and check whether glycine was affecting GlyR-QDs diffusion properties, additional SPT experiments were performed in absence of

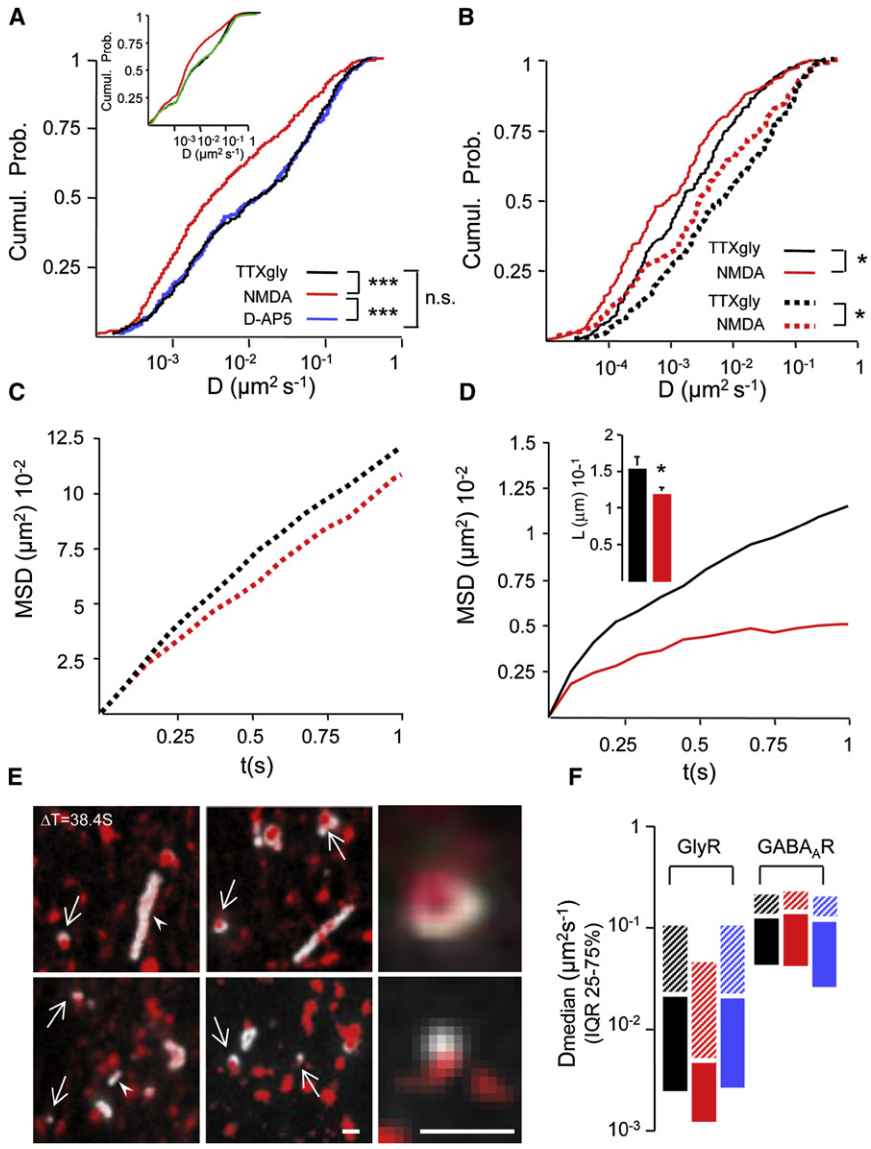

Figure 5. NMDAR Activation Reduces GlyR but Not $GABA_AR$ Lateral Diffusion

(A) Cumulative probabilities of GlyR-QDs diffusion coefficients. NMDA (50 μM) addition in the presence of TTX (1 μM) and glycine (5 μM) (TTXgly condition), significantly decreased GlyR-QDs diffusion coefficients, and this effect was reversed by D-AP5. n.s., not significant; ***$p < 10^{-3}$, KS test. Inset, reversibility of the NMDA effect (20 min, red) after 10 min wash (green) in TTXgly medium. Note that the recovery curve (green) overlaps that obtained before NMDA treatment (black).

(B) Both extrasynaptic (dotted lines) and synaptic (solid lines) GlyR-QDs diffusion coefficients significantly decrease following NMDA addition (red) as compared with TTXgly conditions (black). *$p < 5\ 10^{-2}$, KS test.

(C and D) Average MSD as a function of time of GlyR-QDs at extrasynaptic (C) and synaptic (D) loci. Inset, confinement domain L at synapses (average ± SEM). Note that NMDAR activation increases bending of MSD curves and confinement (*$p < 5\ 10^{-2}$, t test).

(E) Exploration of GlyR-QDs visualized on maximum intensity projections (white) on a 38.4 s recording sequence in TTXgly (upper row) and NMDA (lower row) conditions. FM4-64-stained synapses are red. Right panels show the detail of QD trajectories at synapses, illustrating the increase in confinement. Scale bars, 2 μm. Arrows, QDs at synapses; arrowheads, QDs outside synapses. Note the differences in the explored surface area in TTXgly and NMDA conditions.

(F) Median diffusion coefficients (solid column, ± 25%; hatched column 75% interquartile range, IQR) of GlyR-QDs and $GABA_AR$-QDs. Note that GlyR-QDs but not $GABA_AR$-QDs median diffusion is regulated by NMDAR activity.

In all graphs, QD diffusive behavior in the presence of TTXgly (black), NMDA (red), D-AP5 (blue), or following NMDA reversibility (green).

exogenous glycine. In this condition, we found a significant (3 cultures; $p < 10^{-3}$; KS test) reduction in GlyR-QDs D after exposure to 50 μM NMDA when compared to TTX condition (Figure S7). The curves were superimposable to those obtained in experiments performed in presence of exogenous glycine (5 μM; Figure S7). Therefore, endogenous glycine that could be released by glial cells (Johnson and Ascher, 1987) or present in the culture medium was sufficient for the activation of NMDARs in our culture system.

mIPSCs were recorded using the whole-cell patch-clamp technique in the voltage-clamp configuration. Neurons were treated for 45 min before recording with TTX (1 μM) or with TTX+NMDA (50 μM). Recordings were made in the presence of TTX (1 μM), D-AP5 (50 μM), and NBQX (2 μM) to block action-potential dependent transmission and mEPSCs, and with either SR-95531 (5 μM) or strychnine (1 μM) to isolate glycinergic (Figure 7A) or GABAergic (Figure 7B) mIPSCs, respectively. The isolated glycinergic or GABAergic currents were completely blocked by strychnine or SR-95531 (data not shown). Compared with TTX treatment alone, NMDA addition increased glycinergic but not GABAergic mIPSC amplitude (Figures 7A–7C). This increase in mIPSC amplitude could not be attributed to a change in access resistance between control (12.3 ± 1.2 Mohm) and NMDA (13.1 ± 1.3 Mohm) conditions as it did not change significantly ($p = 0.6$; t test). The average amplitude of glycinergic mIPSCs from NMDA-treated neurons was 161.1% ± 10.7% of that measured in cells maintained in TTX condition (TTX, n = 11, −19.7 ± 1.9 pA; NMDA, n = 10, −29.4 ± 1.7 pA; 3 cultures; $p < 10^{-3}$; t test; Figure 7D). The frequency of glycinergic mIPSCs increased ($p = 0.012$; t test) after NMDA treatment from 2.3 ± 0.9 Hz to 6.1 ± 1.0 Hz (Figure 7E). In contrast, NMDA treatment did not increase GABAergic mIPSC amplitude (TTX, n = 11, −17.5 ± 1.3 pA; NMDA, n = 11, −19.2 ± 1.1 pA; 3 cultures; $p = 0.3$; t test) or frequency (TTX, 1.4 ± 0.2 Hz; NMDA, 1.3 ± 0.2 Hz;

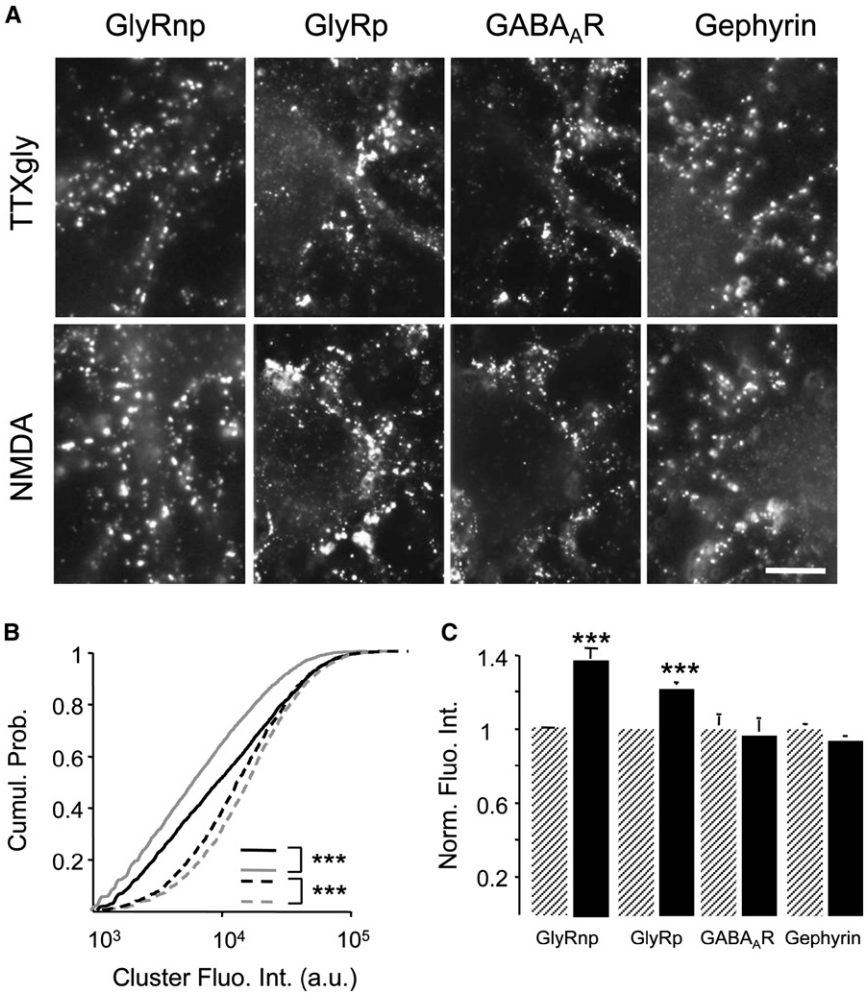

Figure 6. Effects of NMDAR Activation on GlyR, GABA$_A$R, and Gephyrin Cluster Immunoreactivity

(A) Spinal cord neurons at DIV10–13 treated for 2 hr with TTX (1 μM) + glycine (5 μM) TTXgly, TTX + glycine + NMDA (50 μM) NMDA, and stained for the GlyRα1 subunit (GlyRnp, nonpermeabilized cells; GlyRp, permeabilized cells), GABA$_A$Rγ2 subunit, or gephyrin. Scale bar, 10 μm.

(B) Example from one experiment of cumulative distributions of GlyRα1 (solid lines) and GABA$_A$Rγ2 (broken lines) cluster fluorescence intensities in TTXgly (gray) and NMDA (black) conditions. Note that NMDA increases GlyRα1 (***$p < 10^{-3}$, KS test) and slightly decreases GABA$_A$Rγ2 (***$p < 10^{-3}$, KS test) cluster fluorescence intensity. The cumulative distribution for gephyrin cluster fluorescence intensity was slightly decreased as for GABA$_A$Rγ2 after NMDA treatment (data not shown).

(C) Normalized fluorescence intensities (average ± SEM) of GlyRα1np, GlyRα1p, GABA$_A$Rγ2, and gephyrin clusters in TTXgly (hatched) and NMDA conditions (black). Note the significant increase (***$p < 10^{-3}$, t test) in GlyRα1-IR in permeabilized and nonpermeabilized cells after NMDA treatment while GABA$_A$Rγ2- and gephyrin- IR slightly decreased. GlyRα1, GABA$_A$Rγ2, and gephyrin cluster fluorescence intensities were normalized versus the averaged cluster intensity obtained in TTXgly conditions of the corresponding molecules.

p = 0.6; t test; Figures 7F and 7G). Therefore, glycinergic but not GABAergic mIPSCs are increased after NMDAR activation.

Involvement of Ca^{2+} in NMDAR-Dependent Regulation of GlyR Diffusion

Presynaptic release of glutamate can induce Ca^{2+} influx in the postsynaptic cell through the NMDAR channel (Sucher et al., 1996). The involvement of NMDA-dependent Ca^{2+} entry in the regulation of GlyR diffusion was established by comparing the effects of NMDA with or without the extracellular Ca^{2+} chelator EGTA (1.8 mM) on GlyR-QD diffusion. GlyR-QD exploration was increased in the presence of EGTA (Figure 8A, +EGTA). In other words, EGTA inhibited the NMDA-induced decrease in GlyR-QD D. The increase in intracellular Ca^{2+} following NMDAR activation may also result from the activation of IP_3R by IP_3 and modulation by cytosolic Ca^{2+} (Berridge et al., 2003). To determine the involvement of IP_3R-dependent Ca^{2+} release from the endoplasmic reticulum stores in the regulation of GlyR-QD diffusion, cultures were exposed to NMDA condition with or without the cell-permeable IP_3R antagonist 2-aminoethoxydiphenyl borate (2-APB; 100 μM). GlyR-QD exploration was increased (Figure 8A, +2-APB). However, 2-APB also antagonizes the cell membrane-associated store-operated Ca^{2+} entry (SOC) channels (Iwasaki et al., 2001). We found that when the SOC channel inhibitor La^{3+} (100 μM) was added, NMDA still reduced GlyR-QD diffusion, indicating that the SOC channel activation was not responsible for this effect (Figure 8A, +La^{3+}). These effects are quantified in Figures 8B and 8C. The median diffusion coefficients (Figure 8B) emphasize that EGTA and 2-APB but not La^{3+} antagonized the effect of NMDA. These effects on the cumulative distributions were statistically significant (Figure 8C). Therefore, the NMDAR-dependent regulation of GlyR diffusion appears to require calcium influx and release from calcium stores.

DISCUSSION

The main result of this study is that GlyRs and GABA$_A$Rs differ in the regulation of their diffusion properties by activity, leading to changes in GlyR numbers at synapses. First, using single-particle tracking we showed that GlyRs and GABA$_A$Rs diffuse more slowly at mixed inhibitory PSDs than in extrasynaptic membranes. Second, using a pharmacological approach, we found a specific NMDAR-dependent regulation of GlyR but not of GABA$_A$R lateral diffusion, synaptic levels, and mIPSC amplitude. The NMDA-induced changes in GlyR dynamics preceded the changes in the numbers of receptors at synapses. This NMDA-dependent regulation of GlyRs requires calcium influx and release from calcium stores.

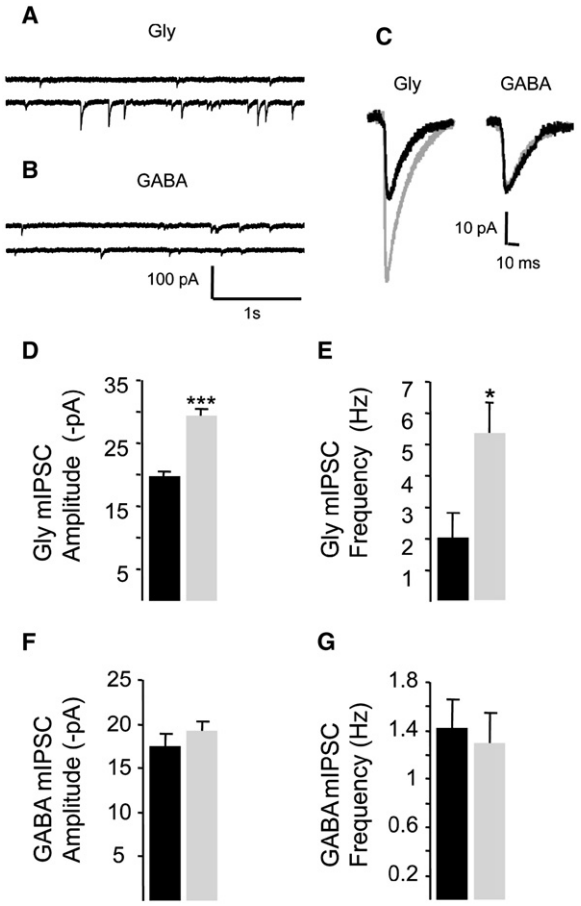

Figure 7. NMDA Treatment Increases Glycinergic but Not GABAergic mIPSC Amplitude

(A and B) Representative recordings of glycinergic (A) and GABAergic (B) mIPSCs in neurons at DIV13 treated with TTX (1 μM, 45 min) (top line) or TTX + NMDA (50 μM) (bottom line) for a holding potential of −70 mV.

(C) Example of traces obtained by averaging 50 glycinergic (left) and GABAergic (right) events recorded from representative neurons treated with TTX (1 μM, 45 min) (black) or TTX + NMDA (50 μM) (gray).

(D and E) Average amplitude (D) and frequency (E) of glycinergic mIPSCs increase following NMDA addition (black) as compared with the TTX condition (hatched). *$p < 5\ 10^{-2}$, ***$p < 10^{-3}$, t test.

(F and G) Absence of NMDA effect on average amplitude (F) and frequency (G) of GABAergic mIPSCs.

In all graphs, values are average ± SEM.

Activity-Dependent Regulation of GlyR but Not of $GABA_AR$ Lateral Diffusion, Synaptic Levels, and Current

Real-time imaging at the single-molecule level has revealed that NTRs are in constant, rapid movement at the neuronal surface and are transiently trapped at the PSD. This is the case for excitatory AMPARs, NMDARs, and mGluRs (Borgdorff and Choquet, 2002; Tardin et al., 2003; Ehlers et al., 2007; Groc et al., 2004; Serge et al., 2002) and for the inhibitory GlyRs (Meier et al., 2001; Dahan et al., 2003; Charrier et al., 2006; Ehrensperger et al., 2007). Here, we showed using SPT that $GABA_ARs$ are also dynamically confined at synapses. The size of the labeling complexes is likely to affect the accessibility of the complexes to the confined synaptic cleft (Groc et al., 2007). However, once a labeled receptor has penetrated the cleft, receptor diffusion is slowed and the measurements of diffusion coefficients reflect genuine properties. The diffusion coefficients and the percentage of immobile AMPAR GluR2 subunits for trajectories measured with single-molecule complexes with different sizes and valences were not significantly different except that the smallest probe allowed the additional characterization of most rapidly diffusing receptors (Groc et al., 2007). The slowing of $GABA_AR$-QDs within synapses is consistent with FRAP and electrophysiological experiments (Jacob et al., 2005; Thomas et al., 2005), two techniques that do not require the use of single-molecule QD complexes. Furthermore, we have previously shown that GlyR-QD dynamics at synapses are similar when measured with CY3 directly coupled to Fab fragments of the GlyR primary Ab (~5 nm) and also with QD-Streptavidin indirectly coupled to Fc fragments of the primary Ab (Dahan et al., 2003). Finally, N-Cam, a transmembrane molecule that does not preferentially accumulate at inhibitory synapses, diffused ~25-fold faster at synapses than GlyR. N-Cam and GlyR were both labeled with QDs. Therefore, QD-receptors can enter and diffuse rapidly within the confined synaptic cleft. In addition, GABAAR-QD diffusion within the synaptic cleft is faster than that of GlyR-QDs. These data and those of others therefore suggest that although QD labeling may affect the entry in the cleft it allows reliable measurements and comparison between various experimental conditions. The fact that N-Cam displayed a higher diffusion and a lower confinement than inhibitory receptors suggested that the slowing and confinement of GlyRs and $GABA_ARs$ at synapses resulted not only from molecular crowding but also from binding to the molecular scaffold (Kusumi et al., 2005; Holcman and Triller, 2006).

We found selective activity-dependent regulation of GlyR but not of $GABA_AR$ lateral diffusion, synaptic receptor numbers, and mIPSC amplitude. Indeed, chronic (24 hr) changes in neuronal activity determine the membrane trafficking and synaptic accumulation of $GABA_AR$ via ubiquitination (Saliba et al., 2007). In short-term treatments (max 2 hr, our experiments), the numbers of $GABA_ARs$ at synapses was not modified. Our results on cultured neurons are consistent with in vivo data (Gonzalez-Forero and Alvarez, 2005) showing that alteration of motoneuron excitatory cholinergic activity decreased glycinergic mIPSC peak amplitude in interconnected Renshaw cells and only weakly affected GABAergic mIPSCs (Gonzalez-Forero and Alvarez, 2005). This resembles the differentiated regulation of NMDARs and AMPARs within individual excitatory PSDs with AMPARs being more dynamic than NMDARs (ref. in Bredt and Nicoll, 2003; Collingridge et al., 2004). KCl-induced depolarization of hippocampal neurons increases AMPAR diffusion (Groc et al., 2004). Inversely, blocking neuronal activity for 48 hr with TTX decreases extrasynaptic AMPAR diffusion. None of these treatments affect NMDAR lateral diffusion in the extrasynaptic and synaptic membranes.

Inhibitory synaptic strength may depend on different GlyR and $GABA_AR$ channel properties. In comparison with $GABA_AR$, GlyR mIPSC rise and decay times are lower (Jonas et al., 1998; Graham et al., 2003). Therefore, glycine and GABA release at a mixed synaptic contact may first induce a large glycinergic current,

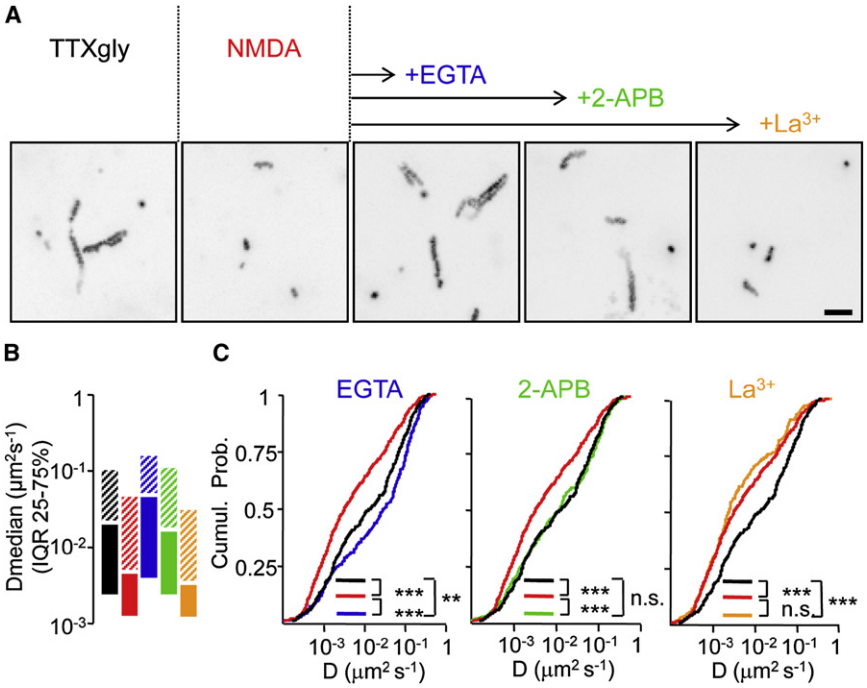

Figure 8. Ca^{2+} Involvement in NMDAR Activation-Dependent GlyR Slow Down

(A) Exploratory maps of GlyR-QDs (black trajectories) visualized on maximum intensity projections of images extracted from a sequence of 512 frames in the presence of TTX (1 μM) + glycine (5 μM) TTXgly, TTX + glycine + NMDA (50 μM) NMDA, TTX + glycine + NMDA + EGTA (1.8 mM), TTX + glycine + NMDA + 2-APB (100 μM), or TTX + glycine + NMDA + La^{3+} (100 μM). Scale bar, 5 μm.

(B and C) Median diffusion coefficients (±25%–75% IQR) (B) and cumulative probabilities (C) of GlyR-QD diffusion coefficients in the plasma membrane in TTXgly (black; D median = 15.5 10^{-3} $\mu m^2 s^{-1}$, n = 493) or NMDA conditions (red; D median = 3.4 10^{-3} $\mu m^2 s^{-1}$, n = 579). The reduction in GlyR mobility following NMDAR activation is reversed by addition of EGTA (blue; D median = 34.6 10^{-3} $\mu m^2 s^{-1}$, n = 341; ***$p < 10^{-3}$, KS test), or 2-APB (green; D median = 12.8 10^{-3} $\mu m^2 s^{-1}$, n = 318; ***$p < 10^{-3}$, KS test), but not after La^{3+} treatment (orange; D median = 2.5 10^{-3} $\mu m^2 s^{-1}$, n = 339; n.s., not significant, KS test). Values are from three cultures.

relayed by a GABAergic current that lasts longer. Favoring regulation of GlyR at mixed glycine-GABA inhibitory synapses is of functional importance in the spinal cord where this receptor predominates in the control of sensory and motor pathways. In other brain areas, where GABA predominates, the number of $GABA_A$Rs is regulated in an activity-dependent manner (Hendry et al., 1994; Otis et al., 1994; Nusser et al., 1998; Kilman et al., 2002). Furthermore, it is now clear that $GABA_A$R clustering is governed by a distinct mechanism in the brain and in the spinal cord.

We found that when excitatory activity was modified, $GABA_A$R diffusion dynamics remained unaffected, and this may help stabilize the subsynaptic scaffold. Indeed, we found that gephyrin abundance at inhibitory synapses was not changed following modification of NMDAR activity. When spinal cord neurons were chronically treated with TTX or with the GlyR antagonist strychnine, GlyR but not gephyrin was removed from the synapse (Levi et al., 1998), leading to the conclusion that at these mixed inhibitory synapses, gephyrin remains associated with $GABA_A$Rs when GlyRs are absent. Conversely, synaptic clustering of $GABA_A$Rs is concomitant with gephyrin and precedes GlyR accumulation at inhibitory synapses (Dumoulin et al., 2000). These data, together with the fact that $GABA_A$R diffusion dynamics are not modified by activity, suggest that $GABA_A$R are involved in the stabilization of the synaptic structure.

Lateral Diffusion as a Tunable Parameter for Synaptic Homeostatic Plasticity

At extrasynaptic loci, GlyR and $GABA_A$R diffusion coefficients were lower than expected for a protein diffusing in an artificial bilayer (ref. in Kusumi et al., 2005). The lateral diffusion of NTRs, like that of many other membrane proteins, is constrained and slowed by a submembranous cytoskeleton meshwork and by immobilized transmembrane proteins. N-Cam, with a short cytoplasmic tail diffused 28- and 20-fold faster than GlyR and $GABA_A$R, respectively. Owing to their bulkier cytoplasmic tails and their larger size than N-Cam, GlyRs and $GABA_A$Rs are restricted in their movements by their greater chance of encountering cytoskeletal barriers. At synapses, the lateral diffusion of NTRs depends both on molecular crowding and interactions with binding sites on scaffold molecules (Meier et al., 2001; Serge et al., 2002; Bats et al., 2007; Ehrensperger et al., 2007). NMDAR activation did not affect N-Cam lateral diffusion in the PSD; therefore, molecular crowding was not modified. In contrast, it decreased GlyR diffusion coefficients and increased its confinement domain. This may result from an increase in the number of scaffolding molecules and/or an increase in receptor-scaffold or scaffold-cytoskeleton interactions. However, since NMDAR activation increased synaptic GlyR abundance without changes in gephyrin-IR, we favor the hypothesis that excitatory activity increases the number of GlyRs at inhibitory PSDs through positive modulation of GlyR and gephyrin interactions rather than by adding gephyrin molecules to the PSD. This regulation is only possible if gephyrin molecules exceed receptors in number at synapses. This is the case for excitatory synapses, since there are ~300 scaffolding molecules in a PSD, whereas the number of NTRs does not exceed 100 (Chen et al., 2005; Cheng et al., 2006; Masugi-Tokita et al., 2007; Sheng and Hoogenraad, 2007). Following synaptic plasticity, itinerant incoming receptors may rapidly occupy free binding sites on subsynaptic scaffold proteins, allowing rapid regulation of the number of receptors at synapses. We have shown that NMDAR-dependent regulation of GlyR membrane diffusion required Ca^{2+} influx and Ca^{2+} release from stores. Receptor-gephyrin interactions could then be enhanced through phosphorylation by Ca^{2+}-dependent kinases. GlyR β subunit and gephyrin contain PKC consensus

sequences (Grenningloh et al., 1990; Prior et al., 1992) and, furthermore, GlyR current amplitude is enhanced by intracellular Ca^{2+} (Fucile et al., 2000) and by phorbol ester activators of PKC (Vaello et al., 1994; Schönrock and Bormann, 1995). One hypothesis is that the NMDAR-dependent calcium signaling pathway increases GlyR or gephyrin phosphorylation, which in turns enhances receptor binding to gephyrin through receptor conformational changes.

Spillover of glutamate released at excitatory synapses may activate extrasynaptic NMDARs (Kullmann et al., 1996; O'Brien et al., 1998) close to inhibitory synapses. This is likely to be the case because on spinal cord neurons that are aspiny, distances between synapses are small (high-density of boutons covering the membrane), and excitatory and inhibitory synapses are intermingled (Ornung et al., 1998). In contrast, AMPARs which are at lower concentrations than NMDARs in the extrasynaptic membrane and accumulate at excitatory synapses (O'Brien et al., 1998) are not implicated in the regulation of GlyR lateral diffusion.

The regulation of inhibitory receptor diffusion dynamics by excitatory input may provide a homeostatic mechanism by which a neuron within a network adapts its inhibition when the excitation is modified during synaptic plasticity. Homeostatic regulation of receptor numbers at synapses has been reported to be a slow process (hours to days) (Turrigiano et al., 1998). Here, we report a rapid and reversible regulation of GlyR dynamics on the order of minutes. Changes in GlyR lateral diffusion preceded modifications in receptor clustering. This can be explained in terms of receptor diffusion dynamics: a "functional pool" of receptors at the synapse is at equilibrium with a "reserve pool" of extrasynaptic receptors (see Triller and Choquet, 2005). Therefore, the activity-dependent balance of receptor entry to and exit from synapses defines the increasing or decreasing number of receptors at synapses. It takes time to change the concentration of receptors at the synapse because the flux is low. Therefore, mobility is likely to be one of the first parameters controlled by ongoing neuronal activity.

In conclusion, our data demonstrate that excitation increases GlyR levels at synapses by a calcium-mediated increase in postsynaptic GlyR trapping, probably through regulation of receptor-scaffold interactions. This provides a mechanism for a rapid homeostatic regulation of the inhibitory glycinergic component at mixed glycine-GABA synapses in response to increased NMDA excitatory transmission.

EXPERIMENTAL PROCEDURES

Primary Neuronal Culture

Cultures of spinal cord neurons were prepared from E14 Sprague-Dawley rats as previously described (Levi et al., 1998). Cells were plated at a density of 5 10^4 cells/cm^2 onto poly-D,L-ornithine (70 μg/ml) and fetal calf serum (10% v/v, Sigma, St Louis, MO) precoated 18 mm diameter glass coverslips (Assistent, Winigor, Germany). Cultures were maintained in serum-free Neurobasal medium with L-glutamine (2 mM) and B27 supplement (1×). Products were from Invitrogen (Cergy Pontoise, France). Cultures were kept at 37°C in 7.5% CO_2 for 10–13 DIV and processed for imaging.

Drug Treatment

The following drugs from Tocris (Avonmouth, UK) were used: TTX (1 μM), strychnine (1 μM), SR-95501 (5 μM), CNQX (50 μM), D-AP5 (50 μM), nifedipine (25 μM), glycine (5 μM), NMDA (50 μM), EGTA (1.8 mM), 2-APB (100 μM), and $LaCl_3$ (100 μM). For immunocytochemistry and electrophysiology, neurons were preincubated for 2 hr or 45 min, respectively, at 37°C with the appropriate drugs directly added to the culture medium. For SPT, neurons were preincubated following QD receptors labeling for 5 min at 37°C with the appropriate drugs in recording medium corresponding to minimum essential medium (MEM) without phenol red supplemented with HEPES buffer (20 mM), glucose (33 mM), glutamine (2 mM), Na^+ pyruvate (1 mM), and B27 supplement (1×). Products were from Invitrogen. Cells were further imaged in recording medium in the presence of the appropriate drugs.

Immunocytochemistry

Cells were fixed for 15 min in paraformaldehyde (PFA, 4% w/v, Serva Feinbiochemica, Heidelberg, Germany) in PBS, and permeabilized for 4 min with Triton X-100 (0.25% v/v). Cells were then incubated for 30 min at 37°C in bovine serum albumin (BSA, 10% w/v, Sigma) in PBS to block nonspecific staining, and incubated for 1 hr at 37°C with primary antibodies in 3% BSA. Following washes with PBS, cells were incubated for 45 min at 37°C with secondary antibodies, washed, and mounted on slides with Vectashield (Vector Laboratories, Burlingame, CA). The primary antibodies used were mouse anti-GlyRα1 subunit (mAb2b; 5 μg/ml; Synaptic System, Göttingen, Germany), mouse anti-gephyrin (mAb7a; 2.5 μg/ml; Synaptic System), rabbit anti-$GABA_AR\gamma2$ subunit (1:200–1:500; Alomone Labs, Jerusalem, Israel), rabbit anti-VIAAT (1:300, gift from B. Gasnier, IBPC, Paris, France), and guinea pig anti-$GABA_AR\gamma2$ subunit (1:2000; gift from J.-M. Fritschy, University of Zurich, Zurich, Switzerland). Secondary antibodies were CY3 conjugated goat anti-mouse, anti-rabbit, or anti-guinea pig (1.33 μg/ml), FITC-conjugated goat anti-mouse or anti-rabbit (3.3 μg/ml), and CY5 conjugated goat anti-rabbit (3.3 μg/ml) from Jackson ImmunoResearch (West Grove, PA). Sets of neurons compared for quantification were fixed, labeled, and imaged simultaneously. For $GABA_AR\gamma2$ labeling, live cells were incubated for 30 min at 37°C with primary antibody from guinea pig (Figure 1) or from rabbit (Figure 6) in conditioned culture medium in the presence of the appropriate drugs. Following washes with conditioned medium, cells were fixed for 15 min in PFA and processed for immunodetection of GlyRα1 alone (Figure 6) or in combination with VIAAT (Figure 1).

Fluorescence Image Acquisition and Analysis

Isolated cells immunoreactive for GlyR or gephyrin were randomly chosen. 12-bit images were acquired with a Micromax CCD camera (Princeton Instruments, Trenton, NJ) on an upright microscope (Leica DMR, 60×, NA 1.3, Nussloch, Germany) using MetaView software (Meta Imaging, Dowington, PA). Exposure time was determined on highly fluorescent cells to avoid pixel saturation. All GlyR, $GABA_AR$, or gephyrin images from a given culture were acquired with the same exposure time. Quantification was performed using MetaMorph software (Meta Imaging). Images were flatten background-filtered (kernel size, 3×3×2) to enhance cluster outlines. A user-defined intensity threshold was applied to select clusters and avoid their coalescence. For the quantification of the proportion of receptors at inhibitory synapses, GlyRα1 and $GABA_AR\gamma2$ clusters comprising at least three pixels and colocalized on at least one pixel with VIAAT clusters were considered.

Calcium Imaging

Neurons at DIV10–12 were loaded with 0.5 μM Fluo-4AM (Invitrogen) for 5 min at 37°C in recording medium. After washing excess dye, cells were further incubated for 5 min to allow hydrolysis of the AM ester. Cells were imaged at room temperature (23°C–24°C) in an open chamber mounted on an inverted microscope (Leica, DM-IRB) equipped with a 63× objective (NA = 1.32, Leica). All washes, incubation steps, and cell imaging were performed in recording medium. Fluo4-AM was detected using a Xe lamp (excitation filter 500 ± 20 nm) and appropriate emission filters (535 ± 30 nm, Omega Opticals, Brattleboro, VT). Time lapse images (10 Hz for 30 s) of Fluo4-AM fluorescence were acquired with a CCD camera (Coolsnap; Princeton Instruments) using Metaview. Fluorescence intensities, collected on proximal dendrites before (F0) and following (F) bath addition of the drugs, were background-subtracted before being displayed as F/F0 values. Data were analyzed using custom-made TI Workbench software (written by T. Inoue, University of Tokyo, Japan).

Live Cell Staining of Inhibitory Receptors for Single-Particle Imaging

Neurons were incubated for 5 min at 37°C with primary antibodies recognizing extracellular epitopes of the GlyRα1 subunit (mAb2b; 2.5 μg/ml), $GABA_AR\gamma2$ subunit (rabbit Ab, 1:200–1:500), or N-Cam (rabbit Ab, 1:2000-1–10,000; gift from R.-M. Mège, IFM, Paris, France), washed, and incubated for 5 min at 37°C with secondary biotinylated Fab antibodies (anti-mouse, 2.8–9 μg/ml; anti-rabbit, 1.7–4.25 μg/ml, Jackson ImmunoResearch). Following washes, coverslips were then incubated for 1 min at 37°C with streptavidin-coated QDs emitting at 605 nm (0.2–0.7 nM, Invitrogen) in borate buffer (50 mM) supplemented with sucrose (200 mM). Following QD labeling and drug treatments, cultures were exposed for 30 s to KCl (40 mM) and FM4-64 (1 μM, Invitrogen) to stimulate synaptic vesicle recycling. Cells were then washed and imaged in the presence of the appropriate drugs. All washes, incubation steps, and cell imaging were performed in recording medium.

Microscopy and Quantum Dot Imaging

Cells were imaged at 37°C in an open chamber mounted on an inverted microscope (Olympus, IX70, Tokyo, Japan) equipped with a 60× objective (NA = 1.45, Olympus). QDs and FM4-64 were detected using an Hg^+ lamp (excitation filter 525DF45) and appropriate emission filters (respectively, 595DF60 and 695AF55, Omega Opticals). Real-time fluorescence images were obtained with an integration time of 75 ms with a CCD camera (Micromax 512EBFT, Roper Scientific), with 512 consecutive frames acquired with Metaview (Meta Imaging). Cells were imaged within 30 min following primary antibody incubation. We have shown that inhibitory receptors are not endocytosed during this recording period. For each SPT experiment, QD dynamics were measured on 12–20 movies from two separate coverslips per culture. In most cases, data were obtained from at least three independent cultures.

Single-Particle Tracking and Analysis

Single-molecule tracking was performed with custom software (Bonneau et al., 2005) using Matlab (The Mathworks Inc., Natick, MA). The center of the fluorescence spots was determined with a Gaussian fit with a spatial resolution of ~10 nm. Single QDs were identified by their blinking property (Alivisatos et al., 2005). Subtrajectories of single QDs with ≥20 points without blinks were retained. Values of the mean square displacement (MSD) plot versus time were calculated for each trajectory with the following relation: $MSD(ndt) = (N-n)^{-1}\sum_{i=1}^{N-n}\left((x_{(i+n)dt}-x_{idt})^2+(y_{(i+n)dt}-y_{idt})^2\right)$ (Saxton and Jacobson, 1997). Diffusion coefficients (D) were calculated by fitting the first five points of the MSD versus time (t) curve with the equation $MSD = 4Dt$. For synaptic trajectories, the size of the confinement domain (L) was obtained by fitting the MSD as follows: $\langle MSD(ndt)\rangle = \frac{L^2}{3}\left(1-\exp\left(\frac{-12D(ndt)}{L^2}\right)\right)$ (Kusumi et al., 1993). L is the side of a square domain in which diffusion is restricted. Spots were classified as synaptic when they overlapped with FM4-64 spots or extrasynaptic for spots at least two pixels (440 nm) distant from the synapse (Dahan et al., 2003).

Electrophysiology

Whole-cell patch-clamp recordings were performed using an Axopatch-1D amplifier. Electrodes had a tip resistance of 4–6 MΩ, when filled with an intracellular solution containing 68 mM KGlu, 68 mM KCl, 0.2 mM EGTA, 2 mM $MgSO_4$, 20 mM HEPES buffer, 3 mM Na_2ATP, and 0.2 mM Na3GTP. All products were from Sigma except HEPES (Invitrogen). The extracellular perfusion medium contained 136 mM NaCl, 2.5 mM KCl, 2 mM $CaCl_2$, 1.3 mM $MgCl_2$ (VWR, Val de Fontenay, France), 10 mM HEPES, and 10 mM D-glucose (Sigma). The medium was supplemented with 1 μM TTX, 50 μM D-AP5, and 2 μM NBQX to isolate mIPSCs. Recordings were filtered at 2–5 kHz and acquired at 5–10 kHz. Currents were recorded in voltage clamp (−70 mV). Throughout the experiment, the access resistance was periodically tested and if it changed by more than 10% or was more than 20 MΩ, the cells were discarded. Data were acquired using the Clampex 10 program and analyzed using the Clampfit 10 program (Axon). mIPSCs were recorded for 1–5 min and averaged in order to obtain the mean amplitude and frequency.

Statistics and Image Preparation

Statistical analyses were performed with StatView (Abacus Concepts, Berkeley, CA) on data compiled and analyzed using Microsoft Excel (Microsoft, Les Ulis, France). Images were prepared for printing using Photoshop (Adobe Systems, San Jose, CA).

SUPPLEMENTAL DATA

The Supplemental Data include seven figures and can be found with this article online at http://www.neuron.org/cgi/content/full/59/2/261/DC1/.

ACKNOWLEDGMENTS

We thank B. Barbour (ENS, Paris, France) for critical reading of the manuscript. The authors are thankful to B. Riveau and C. Ribrault for the supply of primary cultures of spinal cord neurons. We thank J.-M. Fritschy (University of Zurich, Switzerland) for guinea pig γ2 antibody, B. Gasnier (IBPC, Paris, France) for VIAAT antibody, R.-M. Mège (IFM, Paris, France) for N-Cam antibody, and K. Mikoshiba (RIKEN, Japan) for 2-APB. We thank M. Dahan (ENS, Paris, France) and T. Inoue (University of Tokyo, Japan) for the use of their SPT and calcium imaging programs, respectively. This work was supported by the Institut National de la Science et de la Recherche Médicale, the Ministère de la Recherche, the Institut de Recherche sur la Moelle Epinière, the ACI BDP0235, the Sesame convention E. 1762 Région Ile de France, and the Agence Nationale de la Recherche ANR-05-NEUR-043-02. H.B. was supported by Toyobo Biotechnology Foundation, Hayashi Memorial Foundation for Female Natural Scientists, and The Japan Society for the Promotion of Science.

Accepted: May 29, 2008
Published: July 30, 2008

REFERENCES

Alivisatos, A.P., Gu, W., and Larabell, C. (2005). Quantum dots as cellular probes. Annu. Rev. Biomed. Eng. *7*, 55–76.

Bannai, H., Levi, S., Schweizer, C., Dahan, M., and Triller, A. (2006). Imaging the lateral diffusion of membrane molecules with quantum dots. Nat. Protocols *1*, 2628–2634.

Bats, C., Groc, L., and Choquet, D. (2007). The interaction between Stargazin and PSD-95 regulates AMPA receptor surface trafficking. Neuron *53*, 719–734.

Berridge, M.J., Bootman, M.D., and Roderick, H.L. (2003). Calcium signalling: dynamics, homeostasis and remodelling. Nat. Rev. Mol. Cell Biol. *4*, 517–529.

Bredt, D.S., and Nicoll, R.A. (2003). AMPA receptor trafficking at excitatory synapses. Neuron *40*, 361–379.

Bogdanov, Y., Michels, G., Armstrong-Gold, C., Haydon, P.G., Lindstrom, J., Pangalos, M., and Moss, S.J. (2006). Synaptic GABAA receptors are directly recruited from their extrasynaptic counterparts. EMBO J. *25*, 4381–4389.

Bohlhalter, S., Mohler, H., and Fritschy, J.M. (1994). Inhibitory neurotransmission in rat spinal cord: co-localization of glycine- and GABAA-receptors at GABAergic synaptic contacts demonstrated by triple immunofluorescence staining. Brain Res. *642*, 59–69.

Bonneau, S., Dahan, M., and Cohen, L.D. (2005). Single quantum dot tracking based on perceptual grouping using minimal paths in a spatiotemporal volume. IEEE Trans. Image Process. *14*, 1384–1395.

Borgdorff, A.J., and Choquet, D. (2002). Regulation of AMPA receptor lateral movements. Nature *417*, 649–653.

Buller, A.L., Larson, H.C., Schneider, B.E., Beaton, J.A., Morrisett, R.A., and Monaghan, D.T. (1994). The molecular basis of NMDA receptor subtypes: native receptor diversity is predicted by subunit composition. J. Neurosci. *14*, 5471–5484.

Charrier, C., Ehrensperger, M.V., Dahan, M., Levi, S., and Triller, A. (2006). Cytoskeleton regulation of glycine receptor number at synapses and diffusion in the plasma membrane. J. Neurosci. *26*, 8502–8511.

Chen, X., Vinade, L., Leapman, R.D., Petersen, J.D., Nakagawa, T., Phillips, T.M., Sheng, M., and Reese, T.S. (2005). Mass of the postsynaptic density

and enumeration of three key molecules. Proc. Natl. Acad. Sci. USA *102*, 11551–11556.

Cheng, D., Hoogenraad, C.C., Rush, J., Ramm, E., Schlager, M.A., Duong, D.M., Xu, P., Wijayawardana, S.R., Hanfelt, J., Nakagawa, T., et al. (2006). Relative and absolute quantification of postsynaptic density proteome isolated from rat forebrain and cerebellum. Mol. Cell. Proteomics *5*, 1158–1170.

Choquet, D., and Triller, A. (2003). The role of receptor diffusion in the organization of the postsynaptic membrane. Nat. Rev. Neurosci. *4*, 251–265.

Colin, I., Rostaing, P., Augustin, A., and Triller, A. (1998). Localization of components of glycinergic synapses during rat spinal cord development. J. Comp. Neurol. *398*, 359–372.

Collingridge, G.L., Isaac, J.T., and Wang, Y.T. (2004). Receptor trafficking and synaptic plasticity. Nat. Rev. Neurosci. *5*, 952–962.

Dahan, M., Levi, S., Luccardini, C., Rostaing, P., Riveau, B., and Triller, A. (2003). Diffusion dynamics of glycine receptors revealed by single-quantum dot tracking. Science *302*, 442–445.

Dumoulin, A., Levi, S., Riveau, B., Gasnier, B., and Triller, A. (2000). Formation of mixed glycine and GABAergic synapses in cultured spinal cord neurons. Eur. J. Neurosci. *12*, 3883–3892.

Ehlers, M.D., Heine, M., Groc, L., Lee, M.C., and Choquet, D. (2007). Diffusional trapping of GluR1 AMPA receptors by input-specific synaptic activity. Neuron *54*, 447–460.

Ehrensperger, M.V., Hanus, C., Vannier, C., Triller, A., and Dahan, M. (2007). Multiple association states between glycine receptors and gephyrin identified by SPT analysis. Biophys. J. *92*, 3706–3718.

Essrich, C., Lorez, M., Benson, J.A., Fritschy, J.M., and Luscher, B. (1998). Postsynaptic clustering of major GABAA receptor subtypes requires the gamma 2 subunit and gephyrin. Nat. Neurosci. *1*, 563–571.

Feng, G., Tintrup, H., Kirsch, J., Nichol, M.C., Kuhse, J., Betz, H., and Sanes, J.R. (1998). Dual requirement for gephyrin in glycine receptor clustering and molybdoenzyme activity. Science *282*, 1321–1324.

Fucile, S., De Saint Jan, D., de Carvalho, L.P., and Bregestovski, P. (2000). Fast potentiation of glycine receptor channels of intracellular calcium in neurons and transfected cells. Neuron *28*, 571–583.

Gonzalez-Forero, D., and Alvarez, F.J. (2005). Differential postnatal maturation of GABAA, glycine receptor, and mixed synaptic currents in Renshaw cells and ventral spinal interneurons. J. Neurosci. *25*, 2010–2023.

Graham, B.A., Schofield, P.R., Sah, P., and Callister, R.J. (2003). Altered inhibitory synaptic transmission in superficial dorsal horn neurones in spastic and oscillator mice. J. Physiol. *551*, 905–916.

Grenningloh, G., Pribilla, I., Prior, P., Multhaup, G., Beyreuther, K., Taleb, O., and Betz, H. (1990). Cloning and expression of the 58 kd beta subunit of the inhibitory glycine receptor. Neuron *4*, 963–970.

Groc, L., Heine, M., Cognet, L., Brickley, K., Stephenson, F.A., Lounis, B., and Choquet, D. (2004). Differential activity-dependent regulation of the lateral mobilities of AMPA and NMDA receptors. Nat. Neurosci. *7*, 695–696.

Groc, L., Lafourcade, M., Heine, M., Renner, M., Racine, V., Sibarita, J.-B., Lounis, B., Choquet, D., and Cognet, L. (2007). Surface trafficking of neurotransmitter receptor: comparison between single-molecule/quantum dot strategies. J. Neurosci. *27*, 12433–12437.

Hendry, S.H., Huntsman, M.M., Vinuela, A., Mohler, H., de Blas, A.L., and Jones, E.G. (1994). GABAA receptor subunit immunoreactivity in primate visual cortex: distribution in macaques and humans and regulation by visual input in adulthood. J. Neurosci. *14*, 2383–2401.

Holcman, D., and Triller, A. (2006). Modeling synaptic dynamics driven by receptor lateral diffusion. Biophys. J. *91*, 2405–2415.

Iwasaki, H., Mori, Y., Hara, Y., Uchida, K., Zhou, H., and Mikoshiba, K. (2001). 2-Aminoethoxydiphenyl borate (2-APB) inhibits capacitative calcium entry independently of the function of inositol 1,4,5-trisphosphate receptors. Receptors Channels *7*, 429–439.

Jacob, T.C., Bogdanov, Y.D., Magnus, C., Saliba, R.S., Kittler, J.T., Haydon, P.G., and Moss, S.J. (2005). Gephyrin regulates the cell surface dynamics of synaptic GABAA receptors. J. Neurosci. *25*, 10469–10478.

Johnson, J.W., and Ascher, P. (1987). Glycine potentiates the NMDA response in cultured mouse brain neurons. Nature *325*, 529–531.

Jonas, P., Bischofberger, J., and Sandkuhler, J. (1998). Corelease of two fast neurotransmitters at a central synapse. Science *281*, 419–424.

Kilman, V., van Rossum, M.C., and Turrigiano, G.G. (2002). Activity deprivation reduces miniature IPSC amplitude by decreasing the number of postsynaptic GABA(A) receptors clustered at neocortical synapses. J. Neurosci. *22*, 1328–1337.

Kirsch, J., and Betz, H. (1998). Glycine-receptor activation is required for receptor clustering in spinal neurons. Nature *392*, 717–720.

Kirsch, J., Wolters, I., Triller, A., and Betz, H. (1993). Gephyrin antisense oligonucleotides prevent glycine receptor clustering in spinal neurons. Nature *366*, 745–748.

Kneussel, M., Brandstatter, J.H., Laube, B., Stahl, S., Muller, U., and Betz, H. (1999). Loss of postsynaptic GABA(A) receptor clustering in gephyrin-deficient mice. J. Neurosci. *19*, 9289–9297.

Kneussel, M., Brandstatter, J.H., Gasnier, B., Feng, G., Sanes, J.R., and Betz, H. (2001). Gephyrin-independent clustering of postsynaptic GABA(A) receptor subtypes. Mol. Cell. Neurosci. *17*, 973–982.

Kullmann, D.M., Erdemli, G., and Asztely, F. (1996). LTP of AMPA and NMDA receptor-mediated signals: evidence for presynaptic expression and extrasynaptic glutamate spill-over. Neuron *17*, 461–474.

Kusumi, A., Sako, Y., and Yamamoto, M. (1993). Confined lateral diffusion of membrane receptors as studied by single particle tracking (nanovid microscopy). Effects of calcium-induced differentiation in cultured epithelial cells. Biophys. J. *65*, 2021–2040.

Kusumi, A., Nakada, C., Ritchie, K., Murase, K., Suzuki, K., Murakoshi, H., Kasai, R.S., Kondo, J., and Fujiwara, T. (2005). Paradigm shift of the plasma membrane concept from the two-dimensional continuum fluid to the partitioned fluid: high-speed single-molecule tracking of membrane molecules. Annu. Rev. Biophys. Biomol. Struct. *34*, 351–378.

Levi, S., Vannier, C., and Triller, A. (1998). Strychnine-sensitive stabilization of postsynaptic glycine receptor clusters. J. Cell Sci. *111*, 335–345.

Levi, S., Logan, S.M., Tovar, K.R., and Craig, A.-M. (2004). Gephyrin is critical for glycine receptor clustering but not for the formation of functional GABAergic synapses in hippocampal neurons. J. Neurosci. *24*, 207–217.

Masugi-Tokita, M., Tarusawa, E., Watanabe, M., Molnar, E., Fujimoto, K., and Shigemoto, R. (2007). Number and density of AMPA receptors in individual synapses in the rat cerebellum as revealed by SDS-digested freeze-fracture replica labeling. J. Neurosci. *27*, 2135–2144.

Meier, J., Vannier, C., Serge, A., Triller, A., and Choquet, D. (2001). Fast and reversible trapping of surface glycine receptors by gephyrin. Nat. Neurosci. *4*, 253–260.

Muller, E., Le Corronc, H., Triller, A., and Legendre, P. (2006). Developmental dissociation of presynaptic inhibitory neurotransmitter and postsynaptic receptor clustering in the hypoglossal nucleus. Mol. Cell. Neurosci. *32*, 254–273.

Nusser, Z., Hajos, N., Somogyi, P., and Mody, I. (1998). Increased number of synaptic GABA(A) receptors underlies potentiation at hippocampal inhibitory synapses. Nature *395*, 172–177.

O'Brien, R.J., Kamboj, S., Ehlers, M.D., Rosen, K.R., Fischbach, G.D., and Huganir, R.L. (1998). Activity-dependent modulation of synaptic AMPA receptor accumulation. Neuron *21*, 1067–1078.

Ornung, G., Ottersen, O.P., Cullheim, S., and Ulfhake, B. (1998). Distribution of glutamate-, glycine- and GABA-immunoreactive nerve terminals on dendrites in the cat spinal motor nucleus. Exp. Brain Res. *118*, 517–532.

Otis, T.S., De Koninck, Y., and Mody, I. (1994). Lasting potentiation of inhibition is associated with an increased number of gamma-aminobutyric acid type A receptors activated during miniature inhibitory postsynaptic currents. Proc. Natl. Acad. Sci. USA *91*, 7698–7702.

Patneau, D.K., and Mayer, M.L. (1990). Structure-activity relationships for amino acid transmitter candidates acting at N-methyl-D-aspartate and quisqualate receptors. J. Neurosci. *10*, 2385–2399.

Prior, P., Schmitt, B., Grenningloh, G., Pribilla, I., Multhaup, G., Beyreuther, K., Maulet, Y., Werner, P., Langosch, D., Kirsch, J., et al. (1992). Primary structure and alternative splice variants of gephyrin, a putative glycine receptor-tubulin linker protein. Neuron *8*, 1161–1170.

Saliba, R.S., Michels, G., Jacob, T.C., Pangalos, M.N., and Moss, S.J. (2007). Activity-dependent ubiquitination of GABA(A) receptors regulates their accumulation at synaptic sites. J. Neurosci. *27*, 13341–13351.

Saxton, M.J., and Jacobson, K. (1997). Single-particle tracking: applications to membrane dynamics. Annu. Rev. Biophys. Biomol. Struct. *26*, 373–399.

Schönrock, B., and Bormann, J. (1995). Modulation of hippocampal glycine receptor channels by protein kinase C. Neuroreport *6*, 301–304.

Serge, A., Fourgeaud, L., Hemar, A., and Choquet, D. (2002). Receptor activation and homer differentially control the lateral mobility of metabotropic glutamate receptor 5 in the neuronal membrane. J. Neurosci. *22*, 3910–3920.

Sheng, M., and Hoogenraad, C.C. (2007). The postsynaptic architecture of excitatory synapses: a more quantitative view. Annu. Rev. Biochem. *76*, 823–847.

Sucher, N.J., Awobuluyi, M., Choi, Y.B., and Lipton, S.A. (1996). NMDA receptors: from genes to channels. Trends Pharmacol. Sci. *17*, 348–355.

Tardin, C., Cognet, L., Bats, C., Lounis, B., and Choquet, D. (2003). Direct imaging of lateral movements of AMPA receptors inside synapses. EMBO J. *22*, 4656–4665.

Thomas, P., Mortensen, M., Hosie, A.M., and Smart, T.G. (2005). Dynamic mobility of functional GABAA receptors at inhibitory synapses. Nat. Neurosci. *8*, 889–897.

Todd, A.J., Watt, C., Spike, R.C., and Sieghart, W. (1996). Colocalization of GABA, glycine, and their receptors at synapses in the rat spinal cord. J. Neurosci. *16*, 974–982.

Tovar, K.R., and Westbrook, G.L. (2002). Mobile NMDA receptors at hippocampal synapses. Neuron *34*, 255–264.

Tretter, V., Jacob, T.C., Mukherjee, J., Fritschy, J.M., Pangalos, M.N., and Moss, S.J. (2008). The clustering of GABA(A) receptor subtypes at inhibitory synapses is facilitated via the direct binding of receptor alpha2 subunits to gephyrin. J. Neurosci. *28*, 1356–1365.

Triller, A., and Choquet, D. (2005). Surface trafficking of receptors between synaptic and extrasynaptic membranes: and yet they do move! Trends Neurosci. *28*, 133–139.

Turrigiano, G.G., Leslie, K.R., Desai, N.S., Rutherford, L.C., and Nelson, S.B. (1998). Activity-dependent scaling of quantal amplitude in neocortical neurons. Nature *391*, 892–896.

Vaello, M.L., Ruiz-Gomez, A., Lerma, J., and Mayor, F., Jr. (1994). Modulation of inhibitory glycine receptors by phosphorylation by protein kinase C and cAMP-dependent protein kinase. J. Biol. Chem. *269*, 2002–2008.

Wierenga, C.J., and Wadman, W.J. (1999). Miniature inhibitory postsynaptic currents in CA1 pyramidal neurons after kindling epileptogenesis. J. Neurophysiol. *82*, 1352–1362.